Earth beacon acquisition and tracking under various illumination conditions

Barbara Marino*[a], Haiping Tsou**[b], Tsun-Yee Yan[b]
[a]Loyola Marymount University; [b]Jet Propulsion Laboratory

1

ABSTRACT

The use of sun-illuminated Earth images has been explored to aid in meeting the stringent pointing requirements for deep space optical downlink telemetry. It has been shown that fully illuminated Earth images provide a symmetry that easily lends to the determination of the geocenter. Since more often that not, the Earth is only partially illuminated by the sun, more work is required to meet the pointing requirements under all illumination conditions. This paper develops an algorithm for determining the geocenter of the Earth regardless of the illumination by the sun using sub-pixel scanning and a simple thresholding technique. To complete this approach the acquisition algorithm is paired with a tracking technique based on maximum likelihood estimation.

Results have indicated that the algorithm works well to locate and track the position of the Earth and, thereby, a receiving station. Results of the experiments are presented and compared with other techniques.

1. INTRODUCTION

Due to its narrow beam width, deep space optical downlink telemetry requires micro-radian pointing accuracy of the space instruments toward Earth. Many algorithms which use the fully illuminated Earth as a beacon to locate the ground-based telescope have been proposed.[1] Since more often than not, the Earth is only partially illuminated, these algorithms would not be able to meet the pointing requirements for deep space applications.

This paper develops an algorithm for determining the geocenter of the Earth regardless of the illumination angle with the sun. Using a Fine Steering Mirror (FSM) capable of radial movement in increments of 1/20th of a pixel, a sequence of Earth images is taken by scanning in orthogonal directions. The algorithm is based on sub-pixel scans performed first along the Earth-sun axis, and then in the orthogonal direction. To complete this approach the acquisition algorithm is paired with a tracking technique based on maximum likelihood estimation.[2]

Section 2 provides an overview of the mathematical representation of image data at various points in the image capture process. Section 3 describes the acquisition process using sub-pixel scanning, and Section 4 describes the maximum likelihood based tracking of the translated vector. Numerical results demonstrating its capability of sub-pixel acquisition and tracking of fully and partially illuminated Earth images are included in section 5, followed by the summary in section 6.

2. REPRESENTATION OF IMAGE DATA

A block diagram of the process for capturing images for the acquisition and tracking algorithms discussed in this paper is shown in Figure 1. The function $f_l(x,y)$ represents the continuous Earth image at time t_l. The process of capturing this image using an $M \times N$ CCD array is represented by a three-step process. The original image is first convolved with a Gaussian kernel with zero mean and unity variance to represent the degradation introduced by the optics. The intensity of the convolved image is then integrated over the area of each pixel in the CCD array resulting in the extended-source image $s_l(m,n)$. The thermal noise introduced by the CCD array is modeled as an additive white Gaussian random disturbance producing the captured image $r_l(m,n)$, as follows,

$$r_l(m,n) = s_l(m,n) + n_l(m,n), \qquad m = 1,2,\ldots,M, \quad n = 1,2,\ldots,N, \tag{1}$$

where $n_l(m,n)$ is an independent zero-mean Gaussian random variable with variance σ_l^2 for all m and n.

The acquisition algorithm involves subpixel scanning in orthogonal directions. The intensity of a single pixel at location (m,n) is tracked as the FSM is moved in subpixel increments, thereby moving the image across the CCD array. The results of scans in orthogonal directions are denoted, $h_{l,(m,n)}(k)$ and $v_{l,(m,n)}(k)$.

[1]*bmarino@lmu.edu; phone 1 310 338-3947; fax 1 310 338-2782; Loyola Marymount University, Department of Electrical Engineering, 7900 Loyola Boulevard, Los Angeles, CA, USA 90045; **tsou@dsp.jpl.nasa.gov; phone 1 818 354-2393; fax 818 393-1717; Jet Propulsion Laboratory, California Institute of Technology, 4800 Oak Grove Drive, Pasadena, CA, USA 91109

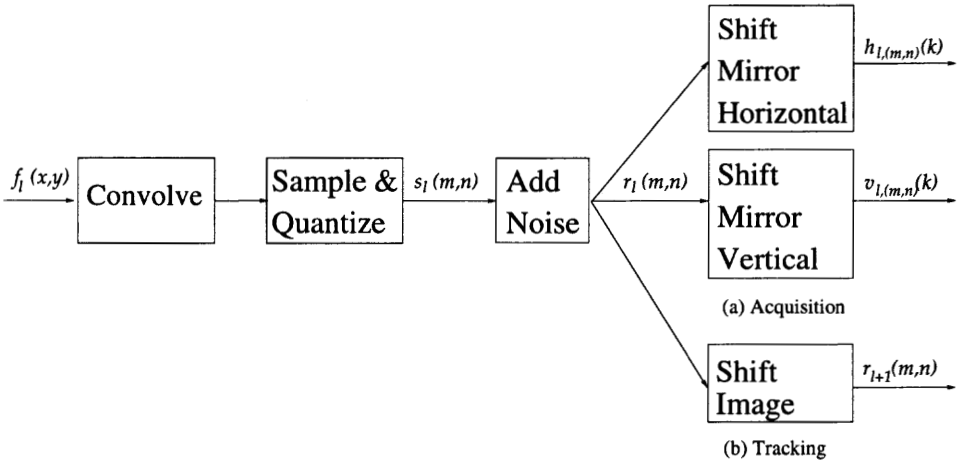

Figure 1. Overview of Data Collection for (a) Acquisition and (b) Tracking Algorithms

The tracking algorithm attempts to quantify change in image location over time. At time, t_{l+1}, the captured image is denoted $r_{l+1}(m,n)$. The tracking algorithm determines the change in location as compared to the reference image geocenter obtained in the above acquisition algorithm.

It is intended to simply provide an introduction to the notation here. The discussion will continue in the following relevant sections.

3. INITIAL ACQUISITION OF EARTH BEACON

3.1. Subpixel Scanning

Subpixel scanning is accomplished by obtaining a sequence of images, $r_l(m,n)$, as the FSM moves the image across the CCD array. Two assumptions are made about the capabilities of the platform. It is assumed that the FSM is capable of radial movement in increments equivalent to 1/20th of a pixel. It is also assumed that the relationship between the positions of the probe, Earth, and sun is known. This information is used to ensure one of the scanning directions is parallel to the Earth-sun axis. This assumption also provides the approximate size of the Earth in pixels as the image is projected on the CCD array. These assumptions are realistic and greatly aid in simplifying the acquisition algorithm.

Using a FSM capable of radial movement in increments of 1/20th of a pixel, a scan is first obtained along the Earth-sun axis, and then in an orthogonal direction. For notational convenience, the Earth-sun axis will be specified as the horizontal direction and the orthogonal direction as the vertical direction.

The history of element (m,n) as the FSM is moved along the horizontal axis at time t_l is represented by the vector $h_{l,(m,n)}$ as follows,

$$h_{l,(m,n)} = \begin{bmatrix} r_l(m,n) \\ r_l(m,n+\frac{1}{20}) \\ \vdots \\ r_l(m,n+\frac{\alpha_N-1}{20}) \end{bmatrix}, \tag{2}$$

where α_N represents the number of samples taken as the mirror is moved in the horizontal direction. Likewise, the history of element (m,n) as the FSM is moved along the vertical axis at time t_l is represented by the vector $v_{l,(m,n)}$ as follows,

$$v_{l,(m,n)} = \begin{bmatrix} r_l(m,n) \\ r_l(m+\frac{1}{20},n) \\ \vdots \\ r_l(m+\frac{\alpha_M-1}{20},n) \end{bmatrix}, \tag{3}$$

where α_M represents the number of scans in the vertical direction. It should be noted that noise introduced in capturing each image, as shown in Eq. (1), is independent of the sub-pixel scanning process.

3.2. Geo-Center Acquisition

The results of sub-pixel scanning provides intensity, and therefore edge, information. Due to the noise introduced by the image capture however, these scans must be smoothed using a low pass filter before edge information can be extracted. This can be easily done in the frequency domain.

The Fourier transform of the horizontal scan at time t_l, becomes

$$\mathcal{H}_{l,(m,n)}(k) = \sum_{p=0}^{\alpha_N - 1} h_{l,(m,n)}(p) e^{-i2\pi\left(\frac{k}{\alpha_N}p\right)}, \quad k = 0, 1, ..., \alpha_{N-1} \tag{4}$$

Applying a low pass filter removes the contributions from frequencies above the cutoff ω_c, and thereby eliminating much of the thermal noise introduced by the CCD array. That is,

$$\widetilde{\mathcal{H}}_{l,(m,n)}(k) = \begin{cases} \mathcal{H}_{l,(m,n)}(k) & \text{when } k < \omega_c, \\ 0 & \textit{otherwise.} \end{cases} \tag{5}$$

The reduced noise time domain signal, $\widetilde{h}_{l,(m,n)}$, may be recovered using the inverse Fourier transform,

$$\widetilde{h}_{l,(m,n)}(k) = \sum_{p=0}^{\alpha_N - 1} \widetilde{\mathcal{H}}_{l,(m,n)}(p) e^{i2\pi\left(\frac{p}{\alpha_N}k\right)}, \quad k = 0, 1, ..., \alpha_{N-1} \tag{6}$$

leaving a smooth time domain representation.

Since the $h_{l,(m,n)}$ and therefore $\widetilde{h}_{l,(m,n)}$ were obtained by scanning in the direction of illumination with the sun, a reliable edge point can be extracted using a simple thresholding edge detection technique. The edge of the Earth is determined by,

$$e_h = \min_k \widetilde{h}_{l,(m,n)}(k) > T, \tag{7}$$

and the horizontal coordinate of the geocenter, x_g,

$$x_g = E_r + e_h, \tag{8}$$

where e_h is the minimum element of the horizontal scan to exceed some threshold, T, and E_r is the radius of the Earth in pixels.

Similarly, Eqs. (4)-(6) can be applied to the vertical scan data, $v_{l,(m,n)}(k)$, to form $\widetilde{v}_{l,(m,n)}(k)$.

With the sun-illumination direction known and specified as the horizontal direction, the Earth image is relatively symmetric in the orthogonal, vertical, direction. The vertical coordinate of the geocenter can be determined from the edge information extracted from the vertical scan, $\widetilde{v}_{l,(m,n)}$. The edges of the Earth in the vertical direction are determined by,

$$e_{v1} = \min_k \widetilde{v}_{l,(m,n)}(k) > T, \tag{9}$$

and,

$$e_{v2} = \max_k \widetilde{v}_{l,(m,n)}(k) > T, \tag{10}$$

and the vertical coordinate of the geocenter, y_g, by,

$$y_g = \frac{e_{v1} + e_{v2}}{2}. \tag{11}$$

4. EXTENDED SOURCE TRACKING OF THE EARTH BEACON

A translation movement within the field of view of the detector array between t_l and t_{l+1} by the amount of x_l and y_l pixels along the x-axis and y-axis can be represented by the following relationship in the 2-D discrete Fourier transform domain

$$\mathcal{S}_{l+1}(m,n) = \mathcal{S}_l(m,n)e^{i\theta_{m,n,l}} \tag{12}$$

where

$$\mathcal{S}_l(m,n) = \sum_{p=1}^{M}\sum_{q=1}^{N} s_l(p,q)e^{-i2\pi\left(\frac{m}{M}p+\frac{n}{N}q\right)} \tag{13}$$

is the transform-domain source image and

$$\theta_{m,n,l} = -2\pi\left(\frac{m}{M}x_l + \frac{n}{N}y_l\right) \tag{14}$$

is the phase introduced to the pixel (m,n) of the transform-domain image due to the translation of coordinate from t_l to t_{l+1}.

A maximum-likelihood-based extended image tracking loop has been developed with the assumption that each pixel of the detected image is corrupted by an independent additive white Gaussian noise. Based on the maximum likelihood criterion, the correlation between the transform-domain received image $\mathcal{R}_{l+1}(m,n)$ and the estimated translated reference image

$$\hat{\mathcal{R}}_{l+1}(m,n) = \mathcal{S}_l(m,n)e^{i\hat{\theta}_{m,n,l}}$$

is to be continuously maximized, rendering the maximum likelihood estimates $\hat{x}_l$ and $\hat{y}_l$ which maximizes

$$\sum_{m=0}^{M-1}\sum_{n=0}^{N-1} Re\left\{\mathcal{R}_{l+1}(m,n)\mathcal{S}_l^*(m,n)e^{-i\hat{\theta}_{m,n,l}}\right\}. \tag{15}$$

Here $\hat{\theta}_{m,n,l}$ is the estimate of $\theta_{m,n,l}$ and the estimation error is

$$\begin{aligned}\phi_{m,n,l} &= \theta_{m,n,l} - \hat{\theta}_{m,n,l} \\ &= -2\pi\left[\frac{m}{M}(x_l - \hat{x}_l) + \frac{n}{N}(y_l - \hat{y}_l)\right] = -2\pi\left(\frac{m}{M}\Delta_x + \frac{n}{N}\Delta_y\right)\end{aligned} \tag{16}$$

where Δ_x and Δ_y are the associated estimate errors. The image tracking loop relies on two loop feedback signals, ε_x and ε_y, formed as the partial derivatives of Eq. (15) with respect to Δ_x and Δ_y, respectively. With a reasonable linear assumption, valid when the phase error $\phi_{m,n,l}$ remains small during the tracking mode, one can substitute Eq. (16) for $\sin(\phi_{m,n,l})$ in ε_x and ε_y. The resulting simultaneous equations are linear for Δ_x and Δ_y and can be easily solved, yielding

$$\Delta_x = \frac{C_n\mathbb{E}[\varepsilon_x] - C_{mn}\mathbb{E}[\varepsilon_y]}{C_mC_n - C_{mn}^2} \tag{17}$$

$$\Delta_y = \frac{C_{mn}\mathbb{E}[\varepsilon_x] - C_m\mathbb{E}[\varepsilon_y]}{C_{mn}^2 - C_mC_n} \tag{18}$$

where $\mathbb{E}[\cdot]$ denotes the statistical expectation and

$$C_m = \frac{4\pi^2}{M^2}\sum_{m=0}^{M-1}\sum_{n=0}^{N-1} m^2|\mathcal{S}_l(m,n)|^2$$

$$C_n = \frac{4\pi^2}{N^2}\sum_{m=0}^{M-1}\sum_{n=0}^{N-1} n^2|\mathcal{S}_l(m,n)|^2$$

$$C_{mn} = \frac{4\pi^2}{MN}\sum_{m=0}^{M-1}\sum_{n=0}^{N-1} mn|\mathcal{S}_l(m,n)|^2$$

are coefficients that can be calculated from the reference image of the previous iteration at t_l.

The subsequent calculation of Δ_x and Δ_y from ε_x and ε_y is straightforward as indicated in Eqs. (17) and (18), except that the statistical averages are replaced by time averages performed by low pass filters. The calculated Δ_x and Δ_y will be used to update the movement estimates through an accumulator, such that

$$\hat{x}_{l+1} = \hat{x}_l + \Delta_x \tag{19}$$

$$\hat{y}_{l+1} = \hat{y}_l + \Delta_y \tag{20}$$

The updated accumulator contents will be used to calculate the estimate $\hat{\theta}_{m,n,l+1}$ and prepare the translated reference image for the next loop iteration at t_{l+1}.

5. RESULTS

The acquisition and tracking algorithms described in this paper have been tested on a number of partially illuminated Earth images. These images, shown in Figure 2, are computer generated images of the Earth as observed from Jupiter during various months of the year 1999. Data from April, October and November are not included because during these months the sun was aligned with the Earth and Jupiter making the Earth indistinguishable from the sun. The remaining images, although mere simulations, provide a wide range of Earth phases while bearing a remarkable similarity to actual images.[5]

The received images, defined in Section 2, are simulated in three steps. The original images are first convolved with a 21 × 21 Gaussian kernel with zero mean and unity variance to represent the degradation introduced by the optics. The images are then scaled to represent the process of image capture assuming a 7 × 7 CCD array. Finally, the images are corrupted by additive white Gaussian disturbances such that the average signal-to-noise ratio,

$$SNR = \sqrt{\frac{1}{MN}\frac{\sum_m \sum_n (s_l(m,n))^2}{\sigma_l^2}}, \tag{21}$$

can be varied. Figure 3 shows this process for the image shown in Figure 2g.

5.1. Acquisition Algorithm

The acquisition algorithm involves scanning the image in two orthogonal directions, capturing a history of the intensity at each element as the FSM moves the image across the CCD array. The result of the horizontal scan, defined in Eq. (2), is a history of α_N samples of the intensity at each pixel location (m,n) as the FSM moves in the horizontal direction. Figure 4 illustrates such a scan across a 7 × 7 CCD array where $\alpha_N = 150$ and $SNR = 10$. Since images are effectively scaled by a factor of 1/20 to represent image capture, and $\alpha_N >> 20$, image information can actually be seen moving from one pixel to another in Figure 4.

The result of the vertical scan, Eq. (3), can be seen in Figure 5. These figures were also generated using Figure 2g, captured on a 7 × 7 CCD array where $\alpha_M = 150$ and $SNR = 10$. In this figure image information can be seen moving from one pixel to another in the vertical direction.

To determine the coordinates of the geocenter, the history at a single pixel location is required, provided the Earth image has completely passed through the location. Figure 6a illustrates the image data collected at CCD element (4,6) during a scan in the horizontal direction. This data is filtered as described in Eqs. (4) - (6), where $\omega_c = 10$. Figure 6a shows the original scan data, the result of low pass filtering, and the application of a threshold, T=3.5, to aid in the determination of the coordinates of the geocenter.

Figure 6b illustrates the image data collected, and the result of low pass filtering, at CCD element (6,3) during the vertical scan. It can be seen that the additive Gaussian noise is practically eliminated by the low pass filtering, making the use of a simple thresholding technique effective.

It bears mentioning that the coordinates of the geocenter can also be determined by considering the history of several pixel locations and a shorter scan of $\alpha_N = \alpha_M = 20$. This approach, however, is not optimal since sensitivity and thermal noise are typically not uniform for all elements in a CCD array. Determining the location of edges using information from two adjacent, yet physically different, CCD elements would introduce unnecessary errors.

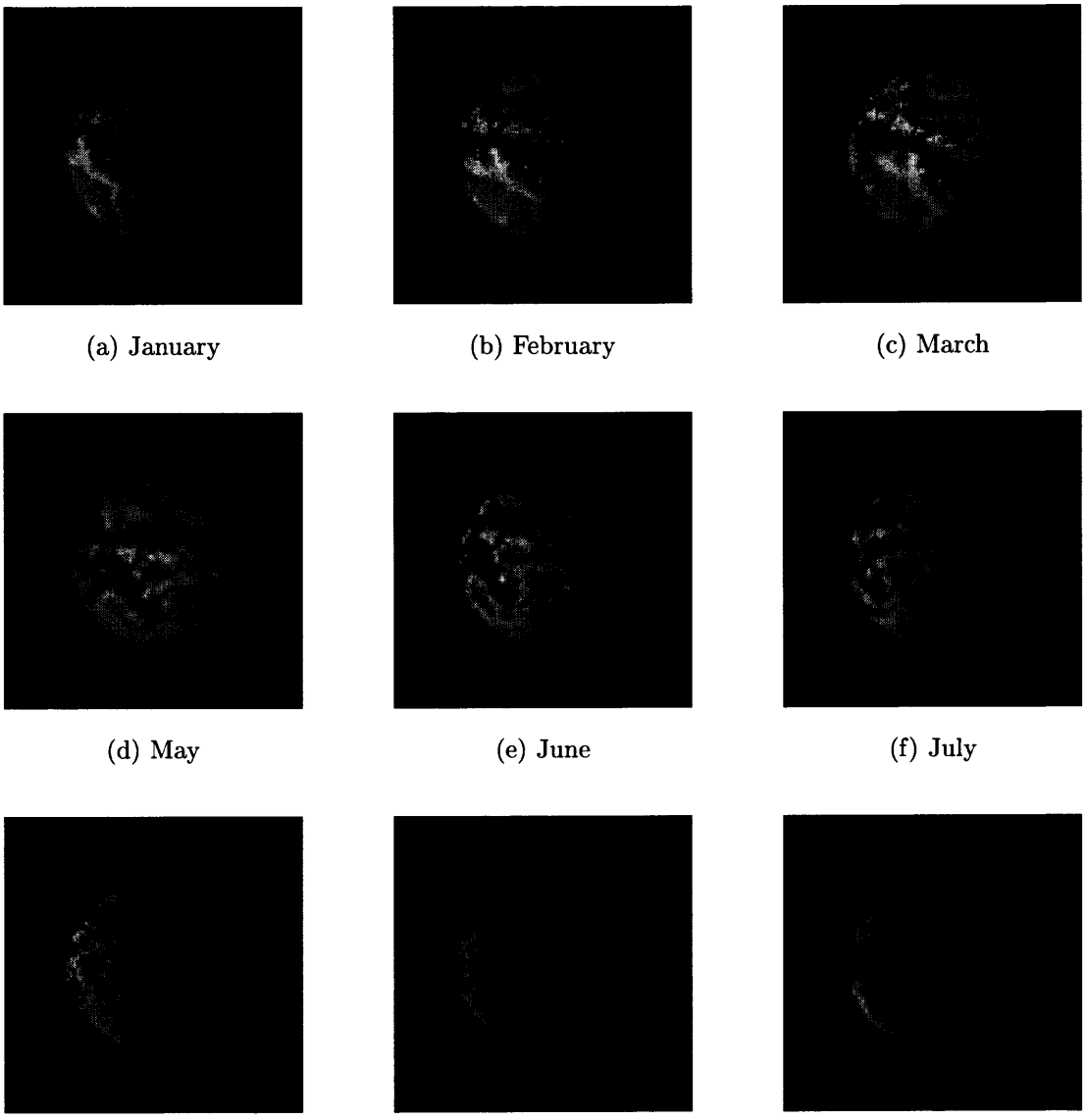

(a) January (b) February (c) March

(d) May (e) June (f) July

(g) August (h) September (i) December

Figure 2. Earth Images Used in Testing Acquisition and Tracking Algorithms.

(a) (b) (c)

Figure 3. Image Capture: (a) Original Image of Size 140 × 140, (b) Smoothed Image of Size 140 × 140, and (c) Detected Image of Size 7 × 7, SNR = 10.

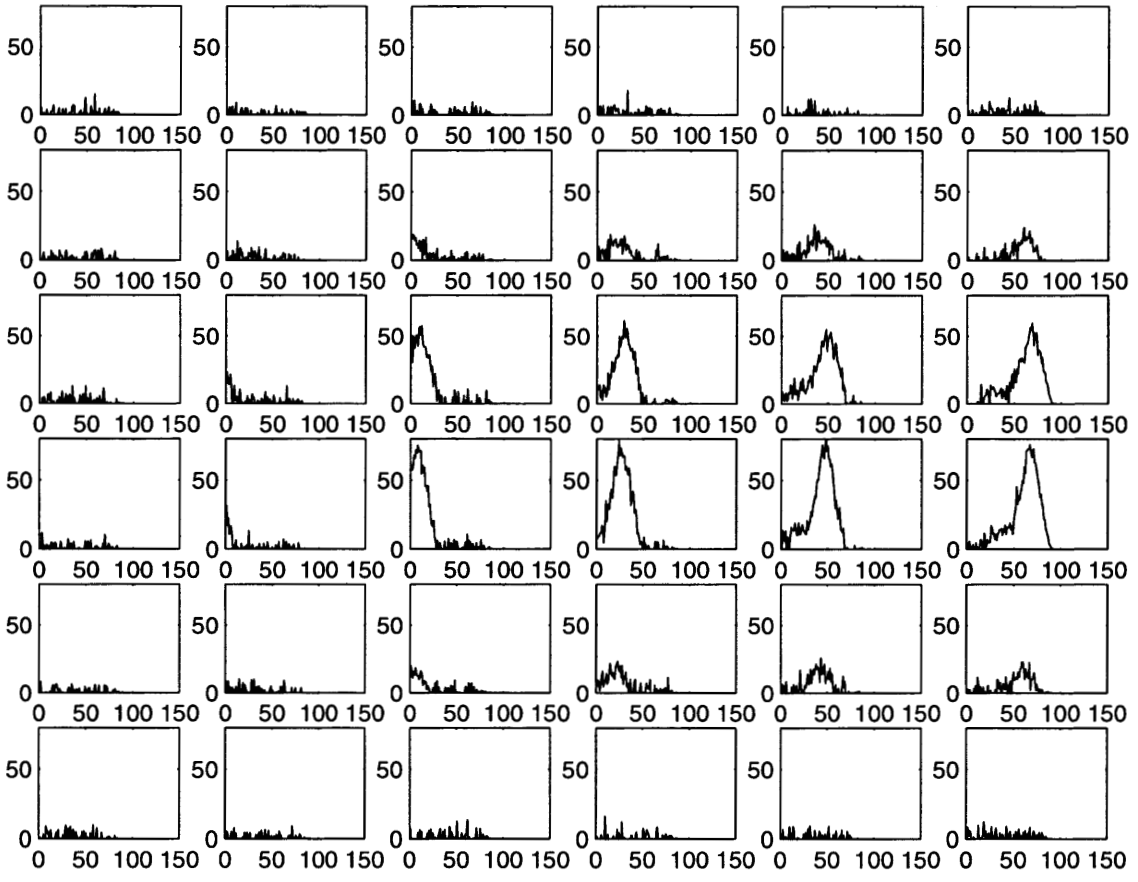

Figure 4. Intensity Profile of Horizontal Scan, h_l

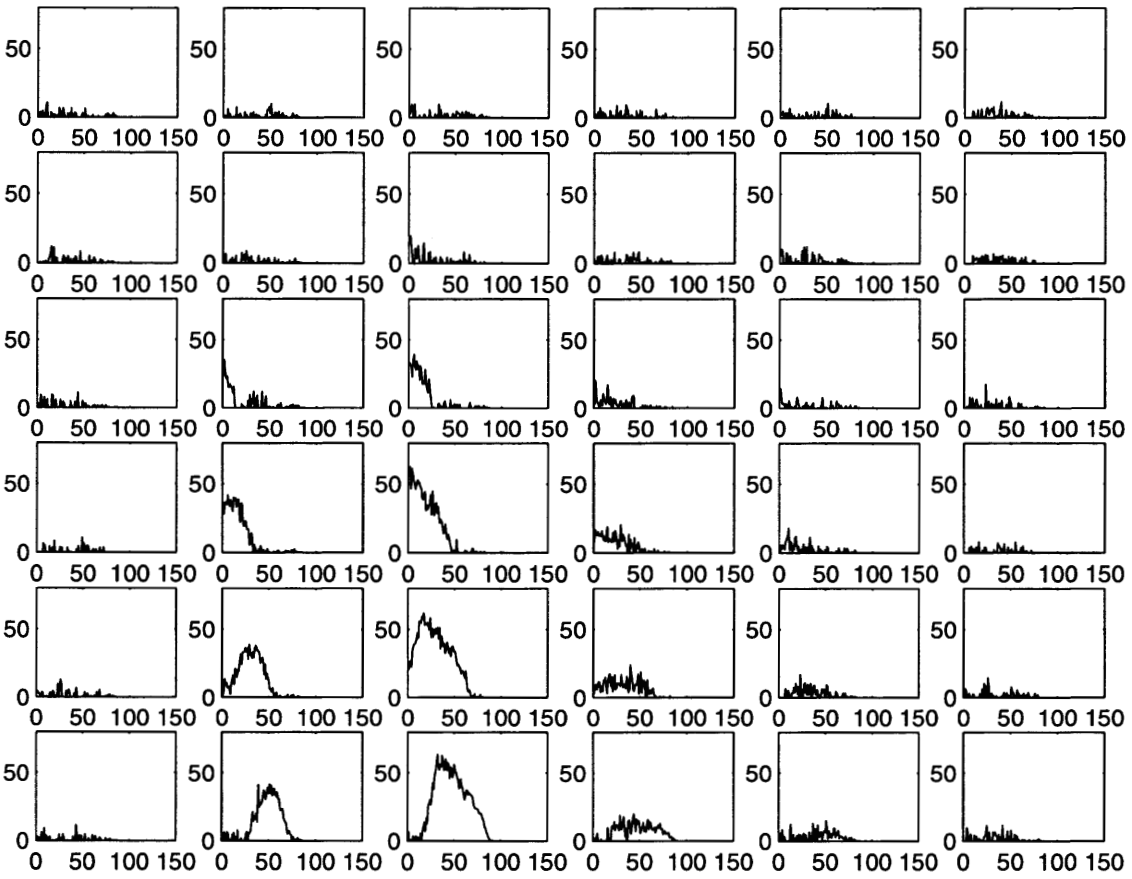

Figure 5. Intensity Profile of Vertical Scan, v_l

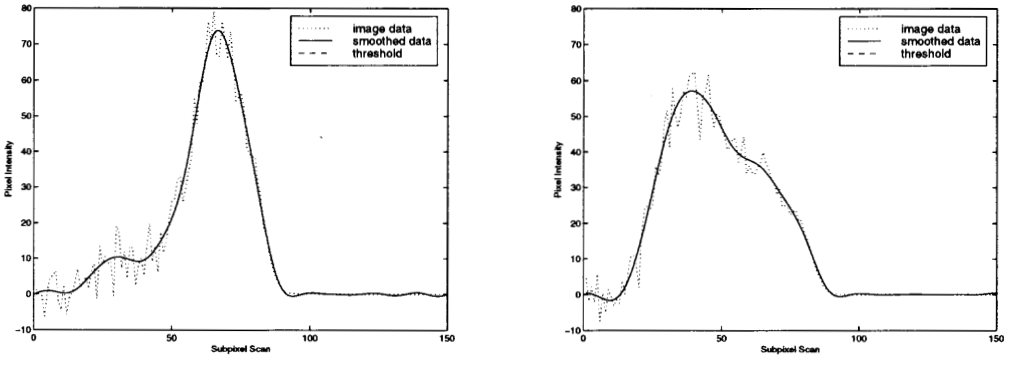

(a) (b)

Figure 6. Subpixel Scanning (a) Horizontal, and (b) Vertical.

Image	Error			
	SNR = 1	SNR = 5	SNR = 10	SNR = 100
January	0.2759	0.1727	0.1428	0.1055
February	0.3122	0.2275	0.1245	0.0140
March	0.4016	0.2519	0.1772	0.0248
May	0.5117	0.3382	0.2915	0.1418
June	0.5448	0.2240	0.1598	0.0641
July	0.3738	0.2037	0.1636	0.1062
August	0.2827	0.1132	0.0639	0.0533
September	0.2425	0.0671	0.0609	0.0650
December	0.2082	0.0930	0.0603	0.0580

Table 1. Results of Acquisition Algorithm Simulations

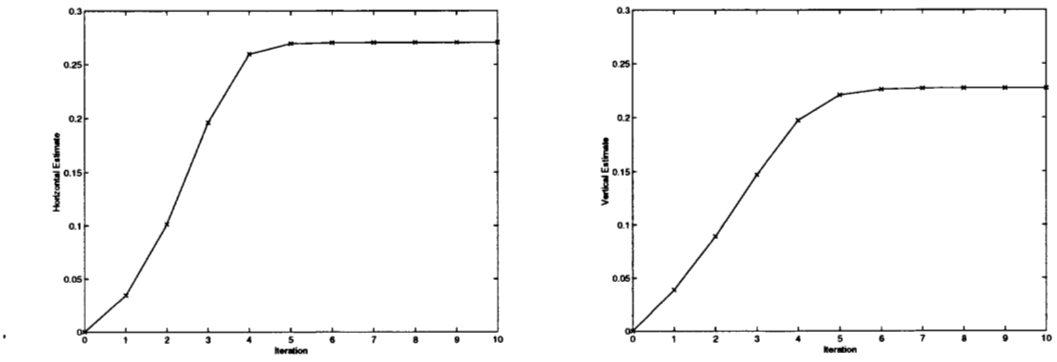

(a) (b)

Figure 7. Tracking (a) Horizontal, and (b) Vertical.

Table 1 quantifies the results of the acquisition algorithm on the various Earth images shown in Figure 2 by averaging the results over ten trials. The error reported is the Euclidean distance of the acquired geocenter from the true geocenter at pixel location $(3, 3)$. These results indicate that the location of the Earth can be acquired for fully and partially illuminated Earth images.

5.2. Tracking Algorithm

The algorithm proposed in Section 4 for tracking is an iterative, closed-loop process in which the feedback is derived from the weighted transform-domain correlation between the received image and the reference image obtained with the acquisition algorithm. Figure 7 illustrates the results of tracking the Earth image of Figure 2g translated by 0.25 pixels in both the horizontal and vertical directions with a signal-to-noise ratio of 10. The results of the first ten iterations are shown, but the solution is often reached in fewer iterations.

Table 2 shows the accuracy of the tracking algorithm averaged over ten trials. The error reported is the Euclidean distance of the estimated translation from the true true translation of 0.25 pixels in both the horizontal and vertical directions. These results indicate that this algorithm can successfully track the movement of the Earth beacon over time for fully and partially illuminated Earth images.

6. CONCLUSION

This paper describes an extended-source spatial acquisition algorithm for planetary optical communications using the sun-lit Earth image as a beacon signal. A sequence of Earth images is taken in two orthogonal directions using a FSM capable of radial movement in the equivalent of 1/20th of a pixel increments. Edge information at sub-pixel resolution is extracted from these scans using a simple thresholding routine. Two assumptions are made to complete the process; it is assumed that the sun-Earth orientation and the expected radius of the Earth image in pixels are

known. Numerical results show that the position of the Earth can be determined with sub-pixel resolution regardless of the observed shape of the Earth, albeto effects or the SNR.

Also described is a tracking scheme which uses the sun-lit Earth image *acquired* using the acquisition algorithm. Since the uncertainties between the reference image and the received image are modeled as additive white Gaussian disturbances, it has been shown that the optimum spatial tracking process derived from the maximum likelihood criterion requires solving two nonlinear equations to estimate the translation vector from the caputured CCD image in the transform domain. An assumption of linearization leads to the closed-loop spatial tracking algorithm in which the loop feedback signals can be derived from the weighted transform-domain correlation between the received image and the reference image. Numerical results of the acquisition and tracking algorithms used in tandem demonstrate that sub-pixel resolutions can be achieved by this maximum-likelihood based spatial tracking scheme in a high disturbance environment.

There are several areas that remain for further investigation. For example, the threshold used in the acquisition algorithm is based on the signal-to-noise ratio. Preliminary work suggests an inverse exponential relationship between the threshold and the signal-to-noise ratio. Future work will attempt to quantify this relationship. Another area left for further study is in characterizing the non-uniformities of the elements in a CCD array. These non-uniformities can perhaps be exploited for improved accuracy.

ACKNOWLEDGMENT

The research described in this paper was carried out by the Jet Propulsion Laboratory, California Institute of Technology under contract with the National Aeronautics and Space Administration.

REFERENCES

1. Shinhak Lee and Tsun-Yee Yan. A Robust Spatial Acquisition Algorithm for Extended Source Using Subpixel Image Scanning. In *Proceedings of the International Conference on Signal Processing Applications & Technology.* 1999.
2. Haiping Tsou and Tsun-Yee Yan. Maximum-Likelihood-Based Extended-Source Spatial Acquisition and Tracking for Planetary Optical Communications. In *Proceedings of the SPIE Conference on Free-Space Laser Communication Technologies XI,* 1999. San Jose, CA.
3. C.D. Kuglin and D. C. Hines. The Phase Correlation Image Alignment Method. In *Proceedings of the International Conference on Cybernetics and Society,* pp. 163-5. 1975.
4. J. J. Pearson, D. C. Hines, S. Golosman, and C. D. Kuglin. Video-rate Image Correlation Processor. In *Proceedings of the SPIE Conference on Application of Digital Image Processing, IOCC,* pp. 197-201. 1977.
5. David Seal. http://space.jpl.nasa.gov/faq.html. 2000.